

Green Synthesis, Characterization and in Vitro Antibacterial Activity of Iron Oxide Nanoparticles Derived from Sandalwood (*Santalum album*) Extract

Vandana Sharma ¹, J. K. Sharma ¹, Vishal Kansay ¹, Varun Dutt Sharma ¹, Mayank Raj ², Manoj Singh ², Anu Kapoor ³, Chhavi Pahwa ¹, Anupam Sharma ⁴, Suresh Kumar ¹, A.K. Sharma ⁵, M. K. Bera ^{1*}

¹ Department of Physics, MM Engineering College, Maharishi Markandeshwar (Deemed to be University), Mullana, Ambala (133207), Haryana, India

² Department of Biotechnology, MM Engineering College, Maharishi Markandeshwar (Deemed to be University), Mullana, Ambala (133207), Haryana, India

³ Department of Physics, Chandigarh University, Gharoun, Mohali (140413), Punjab, India

⁴ MMIS, Maharishi Markandeshwar (Deemed to be University), Mullana, Ambala (133207), Haryana, India

⁵ Department of Biotechnology, Amity University, Mohali (140306), Punjab, India

* Correspondence: m.k.bera@mmumullana.org;

Received: 29.09.2023; Accepted: 15.05.2024; Published: 20.12.2025

Abstract: Green synthesis of iron oxide nanoparticles has recently attracted considerable attention due to its eco-friendly nature, ease of implementation, and excellent biocompatibility. In the present work, nanoscale iron oxide particles have been synthesized at room temperature using ferric chloride hexahydrate in combination with sandalwood (*Santalum album*) extract as a natural reducing agent. The resulting nanoparticles have been thoroughly analyzed using FESEM, EDX, XRD, UV-Vis spectroscopy, FTIR, and VSM techniques. The synthesis yields poly-shaped iron oxide nanoparticles with an average diameter of 42.9 ± 10 nm. Furthermore, a temperature-dependent change in the soft magnetic properties of Fe₂O₃ nanoparticles, with low coercivity and residual magnetism, was observed after calcination. The antibacterial activity of chloramphenicol and streptomycin, along with their formulations encapsulated in iron oxide nanoparticles, is evaluated using the agar well diffusion technique, and the drug-encapsulated nanoparticles demonstrate dose-dependent antibacterial efficacy against *E. coli* and *S. aureus* strains. Chloramphenicol's antibacterial activity has been shown to be significantly improved in the presence of Fe₂O₃ nanoparticles compared to streptomycin.

Keywords: iron oxide nanoparticles; *Santalum album*; green synthesis; antibacterial efficacy; chloramphenicol; streptomycin.

© 2025 by the authors. This article is an open-access article distributed under the terms and conditions of the Creative Commons Attribution (CC BY) license (<https://creativecommons.org/licenses/by/4.0/>), which permits unrestricted use, distribution, and reproduction in any medium, provided the original work is properly cited. The authors retain copyright of their work, and no permission is required from the authors or the publisher to reuse or distribute this article, as long as proper attribution is given to the original source.

1. Introduction

The green chemistry paradigm, which guides the synthesis of biocompatible and functional nanomaterials, aims to innovate by using sustainable processes. Metal and metal oxide nanoparticles (NPs) have been successfully produced using many green synthesis routes [1–6]. Iron oxide NPs are one of the most notable metal oxide NPs among the numerous metals and metal oxide NPs. The outstanding property of iron oxide nanoparticles have broadened their range and applications in medical sciences and a variety of other sectors, including gas sensors, electrochemical, magnetic, and energy storage [7,8]. The superparamagnetic

properties of iron oxide NPs have led to their widespread use in imaging, drug delivery, biosensors, and other applications. Furthermore, their distinct features, including biocompatibility, strong magnetic properties, low toxicity, and catalytic action, have established them as promising candidates for several biological applications [9]. Drug distribution in the form of nanoparticles offers various benefits over traditional drug delivery approaches. Iron oxide nanoparticles in a nanodrug delivery system offer a competitive advantage over other systems due to their outstanding features, including high magnetic properties and a larger, readily adjustable surface area [10–12]. It also enables site-specific drug delivery, helping overcome issues associated with desired bioavailability and facilitating the removal of malignant cells [13]. It has been proven to be a successful method for increasing the therapeutic efficacy of these medications by loading or binding pharmaceuticals using the magnetic and biological properties of iron oxide nanocarriers [14,15]. The majority of drugs exhibit undesirable characteristics, such as low solubility, high toxicity, nonspecific binding, and relatively short circulation half-lives, which can be overcome by conjugation to iron oxide nanoparticles [16]. In addition to their remarkable magnetic properties, iron oxide nanoparticles (Fe₂O₃-NPs) are nontoxic, stable, and environmentally benign, making them an ideal platform for biomedical applications. Additionally, these nanocarriers are safe, biocompatible, biodegradable, and effectively eliminated from the body through iron metabolism [17–19].

Plant extracts, on the other hand, are gaining recognition and support for the synthesis of iron oxide NPs because they can serve as stabilizing and reducing agents during synthesis. Additionally, the biological method for synthesizing iron oxide nanoparticles using plant extract offers several benefits over both physical and chemical methods, including simplicity, affordability, environmental friendliness, and lower energy consumption. Furthermore, the presence of biomolecules on the surface of the NPs, such as flavonoids, alkaloids, terpenoids, and other hydroxyl-containing functional groups, avoids agglomeration and facilitates the production of NPs with uniform particle size [20,21].

In this work, we report the synthesis of iron oxide nanoparticles (Fe₂O₃ NPs) using iron tetrachloride hexahydrate as a precursor and various phytochemicals from sandalwood (*Santalum album*) extract as reducing and capping agents. Various physicochemical, morphological, structural, surface functional, optical, and magnetic properties have been investigated. Nanoformulated antibiotics, such as chloramphenicol and streptomycin, conjugated to iron oxide nanoparticles, were further investigated for in vitro antimicrobial activity.

2. Materials and Methods

2.1. Materials.

Ferric chloride hexahydrate (FeCl₃ · 6H₂O) and sodium hydroxide (NaOH) were purchased from Sisco Research Laboratories Pvt. Ltd. (India) and used without further purification. Whatman filter paper (grade 1), acetone, ethanol, and isopropyl alcohol were all purchased from a commercial provider. A Milli-Q system (18.2 MΩ.cm, Millipore, France) was used to acquire double-distilled water.

2.2. Green synthesis of iron oxide nanoparticles.

Sandalwood (*Santalum album*) was purchased at a local market. To eliminate dust particles, the sandalwood was carefully washed with DI water. After washing, the sandalwood

was dried in an oven at 60°C for 24 hours. After grinding the sandalwood into a fine powder, a 1000 ppm extract solution was prepared. After half an hour of settling, the extract was filtered twice through Whatman No. 1 filter paper. Ferric chloride hexahydrate was used as a precursor in the synthesis of the Fe₂O₃ NPs. To begin, a homogenous 0.1 M ferric chloride solution was made by dissolving it in deionized water under constant stirring at room temperature. The *Santalum album* extract solution was then added in a volumetric ratio of 1:1 to the ferric chloride solution at room temperature. 1 M NaOH was added dropwise with continuous stirring to elevate the pH of the solution to 12, resulting in a black precipitate. The stirring was maintained at 600 rpm to complete the reaction. It was then maintained for a couple of hours to stabilize. The precipitate was removed from the solution by centrifuging it at 6000 rpm for 10 minutes. The resultant Fe₂O₃-NPs were then carefully washed with distilled water multiple times before being dried for an extended period in a hot-air oven. The NPs were calcined in a hot furnace for 3 hours at two different temperatures, 500 and 700°C. The dried Fe₂O₃-NP powder was used for further investigation and physical characterization.

2.3. Characterizations and instrumentations.

The sample was ultra-centrifuged using a REMI CPR-30 Plus centrifuge. The UV-Vis absorption spectra were collected using a Shimadzu UV-2600 spectrophotometer with a 1 nm step in the wavelength range 200-800 nm. The mixture was stirred using a REMI MS-500 magnetic stirrer. A Shimadzu IR-Spirit Fourier transform infrared (FTIR) spectrophotometer in the wavelength range 4000-400 cm⁻¹ was used to determine the type of surface functionalization. Using a Bruker D8 Advance diffractometer at 40 kV, 40 mA, and a non-monochromatic Cu K_α X-ray with an angular range of 5-90° and an angular step of 0.02°, the crystalline character of the NPs was confirmed. The morphologies of synthesized NPs were examined with a Zeiss field-enhanced secondary electron microscope (FESEM) set to 5 kV. The composition of Fe₂O₃-NPs was determined using energy-dispersive X-ray spectroscopy (EDX). At room temperature, magnetization was measured using a vibrating sample magnetometer (VSM-7404, Lake Shore, USA).

2.4. Bacterial reduction assay.

Microbial assays were used to evaluate the effectiveness of the investigated iron oxide-coated antibiotics (chloramphenicol and streptomycin) by comparing the growth inhibition of sensitive bacteria produced by known amounts of the test antibiotic and a reference drug. In this study, gram-negative and gram-positive bacteria, *E. coli* and *S. aureus*, respectively, were cultured in nutrient broth overnight at 37°C for 24 hours to study bacterial growth. A spectrophotometer was used to measure the optical density at 620 nm to evaluate bacterial growth curves [22].

2.5. Preparation of antibiotic-coated iron oxide nanoparticles.

The use of nanomedicine to deliver antibiotics can improve the efficacy of antibacterial treatment. Compared with traditional formulations, nanosystems for antibiotic administration and infection-site targeting offer several benefits. Antibiotic-coated Fe₂O₃-NPs were prepared to investigate the role of nanoparticles in microbial activity. Firstly, in order to assess the combined impact of each standard antibiotic, 10-30 μL of freshly synthesized Fe₂O₃-NPs (calcinated @ 500°C) was mixed. Chloramphenicol and streptomycin were the two medicines

employed in this investigation. *S. aureus* and *E. coli* were the bacterial isolates employed in this study.

2.6. Microbial assay.

The in vitro antibacterial activity of chloramphenicol and streptomycin, as well as their combination effect with Fe₂O₃-NPs, was assessed for this purpose using the well diffusion technique on Mueller-Hinton agar plates. Initially, a spore suspension (20 μL) of the tested bacteria was inoculated onto Mueller-Hinton agar plates. Drug-coated Fe₂O₃-NPs were then placed on agar plates and incubated at 25°C for at least 1 hour to allow pre-incubation diffusion and reduce the effect of time differences when different solutions were used. After 12-24 hours of incubation at 37°C, the plates were examined for antibacterial activity by measuring the width of the inhibition zones for each bacterial culture [22].

2.7. Assessment of increase in fold area.

The mean surface area of the inhibitory zone for pure drugs and Fe₂O₃-NP-coated drugs was evaluated to estimate the fold increase in surface area. The fold increase in area of each examined microorganism was computed using the equation:

$$(P^2 - Q^2)/P^2 \quad (1)$$

Where P and Q were the zones of inhibition for prescribed drugs and drugs coated with iron oxide nanoparticles, respectively [22].

3. Results and Discussion

3.1. Morphological, compositional, structural, and chemical characteristics of *Santalum album*-derived Fe₂O₃-NPs.

The morphology of the synthesized Fe₂O₃-NPs as obtained by FESEM is shown in Figure 1a. The FESEM image clearly shows that the synthesized iron oxide nanoparticles are not uniform and can occasionally aggregate. The particles are found to be polygonal in nature with a size distribution within the range of 42.9±10 nm (inset of Figure 1a). The observed massive agglomerated clusters were most likely generated as a result of a high surface area to volume ratio, strong dipole-dipole interactions, van der Waals attractive forces, or magnetic forces.

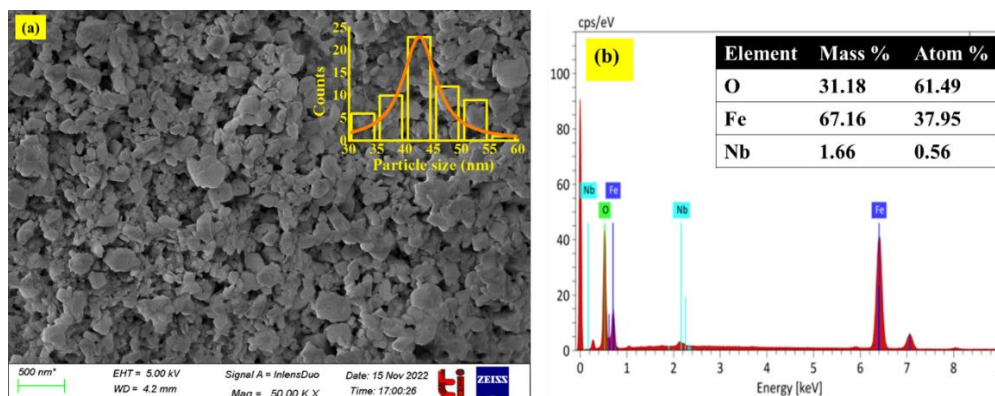


Figure 1. (a) FESEM micrograph of iron oxide nanoparticles (Fe₂O₃-NPs) synthesized from *Santalum album* extract (calcinated at 500°C in air). The inset figure shows the Fe₂O₃-NPs size distribution histogram; (b) Compositional analysis by EDX spectra.

Furthermore, because of the high surface area-to-volume ratio, strong dipole-dipole interactions, van der Waals attractive forces, and magnetic forces, magnetic nanoparticles clump together and form large clusters, increasing particle size. The elemental composition of the Fe₂O₃-NPs was also determined via EDX analysis. The EDX analysis shown in Fig. 1b clearly demonstrates the existence of corresponding L_{α} at 0.7 keV, K_{α} at about 6.4 keV, and another K_{α} line at 0.6 keV due to the presence of O atoms in the nanoparticle. According to the table in Fig. 1b, the fraction of iron and oxygen atoms in the irradiated area is 37.95 at. % and 61.49 at. %, respectively. The presence of niobium (Nb) at a trace level (0.56 at.%) is most likely due to minerals in *Santalum album*. It is indeed important to remember that the carbon observed in EDX spectra (K_{α} at 0.2 keV) may arise from air or from interactions with organic molecules during preparation. Any organic contamination tends to produce hydrocarbons on the sample surface beneath the electron beam, and their amount may increase throughout the experiment. Hence, EDX analysis indicates that Fe₂O₃ NPs were successfully synthesized using *Santalum album* in a green synthesis process.

The structural properties of *Santalum album*-derived Fe₂O₃-NPs were characterized by XRD. Figure 2a shows the XRD patterns of as-synthesized and 500°C and 700°C calcinated samples. X-ray diffraction reveals that the calcinated samples (either 500 or 700°C) demonstrated the development of polycrystalline iron oxide nanoparticles with strong peaks from the (104), (110), (024), (116), (214) and (300) planes (JCPDS: 01-080-2377), whereas the nascent sample suffered from crystallization. The strong peaks of nanoparticles rather illustrate the good crystallinity of calcinated samples. However, the presence of Fe₃O₄ and γ -Fe₂O₃ cannot be detected by XRD because magnetite and maghemite have almost similar crystal structures [23].

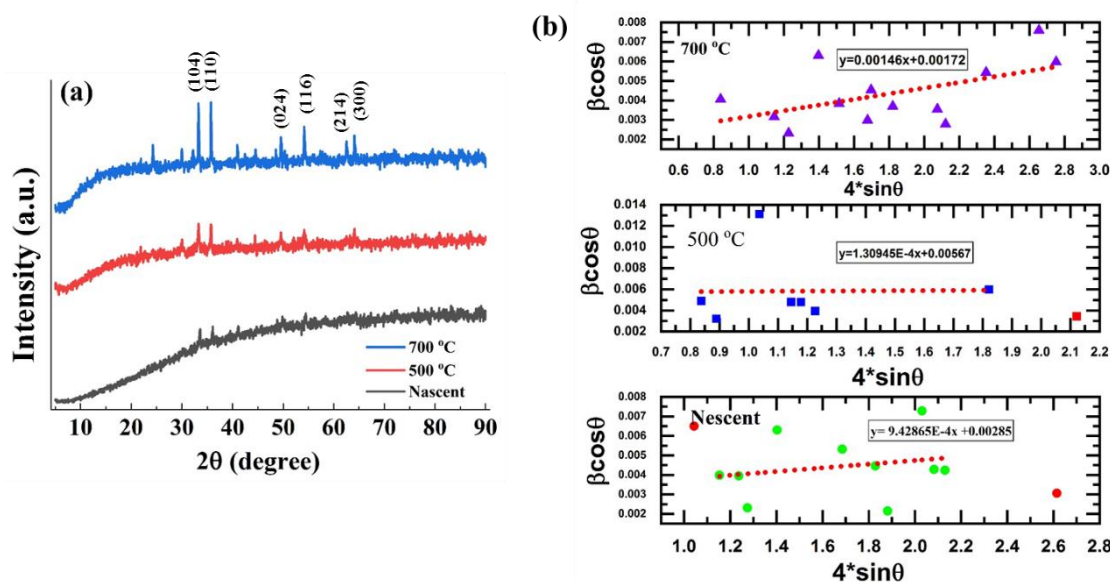


Figure 2. (a) XRD patterns; (b) Williamson-Hall plot of the *Santalum album*-derived iron oxide nanoparticles.

The three most common types of iron oxides found in nature are magnetite (Fe₃O₄), maghemite (γ -Fe₂O₃), and hematite (α -Fe₂O₃); however, XRD makes distinguishing the presence of magnetite (Fe₃O₄) and maghemite (γ -Fe₂O₃) difficult because magnetite and maghemite have nearly identical crystal structures. Among these crystalline phases, hematite is the most stable form of iron oxide. Chemical co-precipitation, hydrothermal synthesis, and the sol-gel technique are common methods for producing hematite nanoparticles [24]. These nanoparticles' particle size and shape may be easily adjusted by changing numerous factors related to their production technique.

Using the prominent peaks from Debye-Scherrer's formula, the average crystallite size (d_{np}) was computed [13]:

$$d_{np} = \frac{\kappa\lambda}{\beta\cos\theta} \quad (2)$$

Where $\lambda=0.15406$ nm is the wavelength of $\text{CuK}\alpha$ radiation, β is the full width at half maxima (FWHM) of the diffraction peak in radians, and θ is Bragg's diffraction angle, κ is a constant (0.9 for spherical shape), respectively. The average crystallite size was determined to be about 21.9 nm. Additionally, the Williamson-Hall (W-H) plot and the following relationship were used to calculate the lattice strain from the FWHM of the diffraction peaks [23]:

$$\beta\cos\theta = \frac{\kappa\lambda}{d_{np}} + 4\varepsilon\sin\theta \quad (3)$$

Where ε denotes the effective strain. Plotting the term ($\beta\cos\theta$) with respect to ($4\sin\theta$) for the preferred orientation peaks of Fe_2O_3 -NPs yields the size and associated strain of the crystallites as well as the fitted line's y-intercept and slope, respectively [25,26]. The W-H plots for nascent and calcinated Fe_2O_3 -NPs, as shown in Figure 2b, demonstrate that the strain is exceedingly small.

In addition, FTIR spectra were used to identify functional groups and confirm the formation of Fe_2O_3 -NPs in the produced samples. Figure 3 depicts the FTIR spectra of as-prepared and calcined Fe_2O_3 -NPs. The existence of distinct reducing agent functional groups connected with Fe_2O_3 -NPs was established by FTIR analysis ($400\text{-}4000\text{ cm}^{-1}$) of all samples (nascent and calcinated samples).

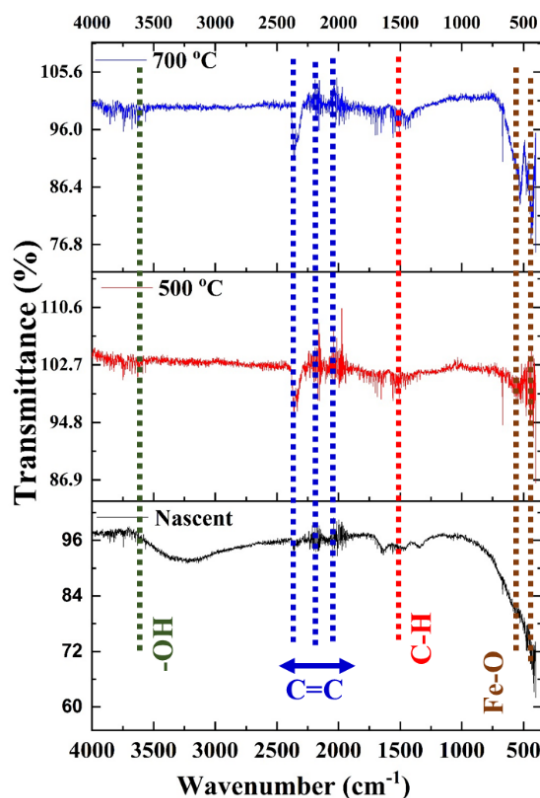


Figure 3. FTIR spectra of *Santalum album*-derived iron oxide nanoparticles.

The spectra of Fe_2O_3 -NPs exhibit a distinct band at 570 cm^{-1} , which is associated with iron oxide's Fe-O vibrations [27]. Other stretching vibrations have been seen at the following frequencies: 2363 cm^{-1} (O=C=O), 2166 cm^{-1} (N=C=N), 2070 cm^{-1} (C=C), 1955 cm^{-1} (C=C=C), and 1754 cm^{-1} (C=O) [28,29].

3.2. Optical characteristics of *Santalum album*-derived Fe₂O₃-NPs.

The absorbance spectra of nascent and calcinated iron oxide nanoparticles are shown in Figure 4. The indirect optical bandgap is evident from the gradual absorbance peaks in the 550-800 nm range [30].

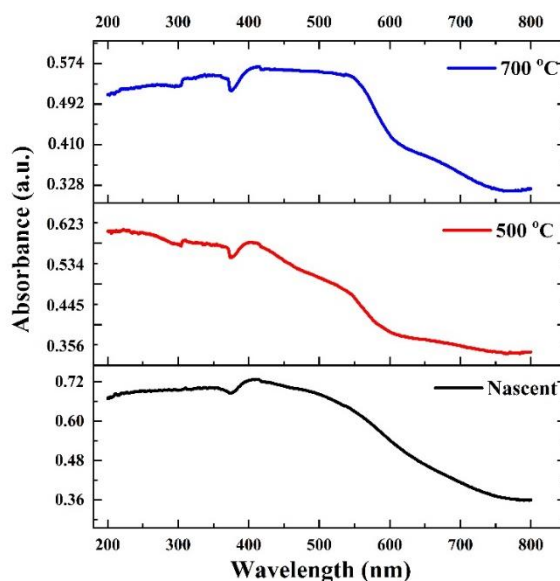


Figure 4. UV-Vis absorption spectra of iron oxide nanoparticles synthesized from *Santalum album* extract. The influence of calcination temperature is also shown.

The Tauc method, which is based on the premise that the energy-dependent absorption coefficient may be given by the following equation, is frequently used to estimate the bandgap [31]:

$$(\alpha h\nu)^{1/\gamma} = B(h\nu - E_g) \quad (4)$$

Where, ν is the photon's frequency, E_g is the band gap energy, h is the Planck constant, and B is a constant. The γ factor is determined by the type of electron transition and is equal to 1/2 or 2 for direct and indirect transition band gaps [31]. The Tauc plot of nascent and calcinated Fe₂O₃-NPs samples is shown in Figure 5. It has been observed that the indirect band gap decreases consistently as the calcination temperature rises (1.2 eV for nascent vs. 0.975 eV for 500°C or 0.95 eV for 700°C).

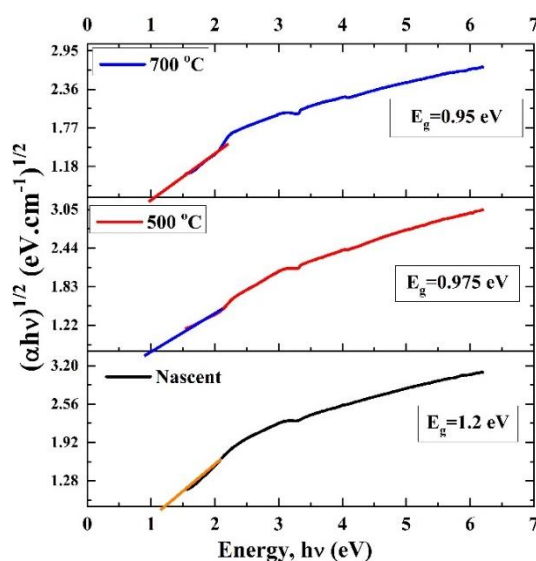


Figure 5. Estimation of bandgap from Tauc plot using the UV-Vis absorption spectra of iron oxide nanoparticles synthesized from *Santalum album* extract.

3.3. Magnetization measurement *Santalum album* derived Fe₂O₃-NPs.

Magnetic hysteresis (M-H) loop measurements at room temperature (300 K) were carried out with a vibrating sample magnetometer (VSM) equipped with a Lake Shore model 7404 and a maximum applied field of 1 T. Figure 6 depicts a typical M-H loop of nascent and Fe₂O₃-NPs powder calcined at 500°C and 700°C. The distinctive hysteresis loop demonstrates that powders are magnetic in nature. All samples exhibit observable coercivity (H_c) and residual magnetism (M_r) (inset of Fig. 6), confirming ferromagnetic ordering.

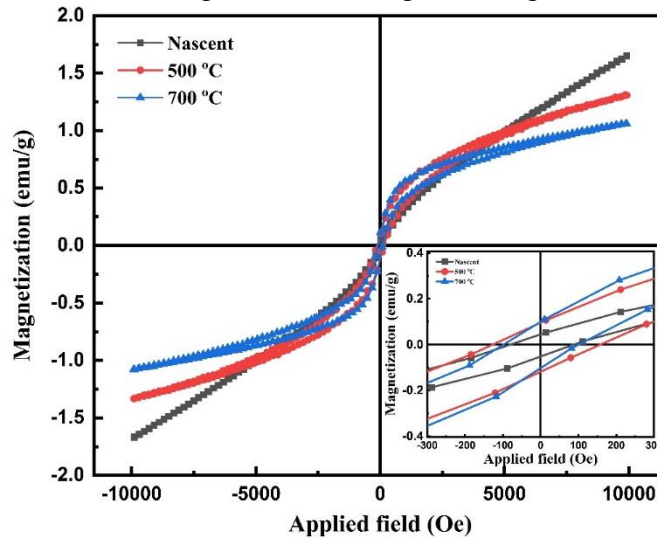


Figure 6. *M–H* loops of nascent and calcinated (500 and 700°C) iron oxide nanoparticles (Fe₂O₃-NPs) synthesized from *Santalum album* extract. The inset shows the magnified view of the *M–H* loop.

The relatively low coercivity (less than 1000 Oe) and Mr (see Table 1) confirm the (Fe₂O₃) material's soft magnetic nature. The increased M_r and H_c of calcinated samples compared to nascent samples demonstrated that H_c and M_r are predominantly influenced by extrinsic factors, such as nanoparticle crystallite size and form, which are predicted to decrease as the calcination temperature rises. Therefore, the fluctuation in M_r and H_c demonstrates that magnetic characteristics vary with calcination temperature.

Table 1. Magnetic properties (*M_s*, *M_r*, and *H_c*) of nascent and calcinated *Santalum album*-derived Fe₂O₃-NPs.

Sample	<i>M_s</i> (emu/g)	<i>M_r</i> (emu/g)	<i>H_c</i> (Oe)
Nascent	1.65	0.05	82
500°C	1.31	0.12	148
700°C	1.06	0.1	104

3.4. Bacterial growth inhibition assay and drug delivery applications of Fe₂O₃-NPs.

A bacterial reduction assay was used to examine the in vitro antibacterial effects of iron oxide nanoparticles against multidrug-resistant strains of Gram-negative (*E. coli*) and Gram-positive (*S. aureus*) bacteria at various time points (1-24 hrs) and concentrations (10-30 μL). Figure 7(a) shows digital photographs of the antibacterial study of chloramphenicol-loaded iron oxide nanoparticles (10 μL).

Figure 7(b) shows that the antibacterial activity was significantly improved when chloramphenicol-encapsulated Fe₂O₃ NPs were used as drug carriers compared to chloramphenicol or NPs alone, mainly because it is essentially a compound consisting of closely related aminoglycosides and a group of antimicrobial agents that normally inhibit protein synthesis. The inhibition of protein synthesis or genetic translation is the main

mechanism of action of these drugs. Phospholipids are created when iron and gentamycin are combined [32]. The sulfate group forms a covalent bond, coating the nanoparticles [33].

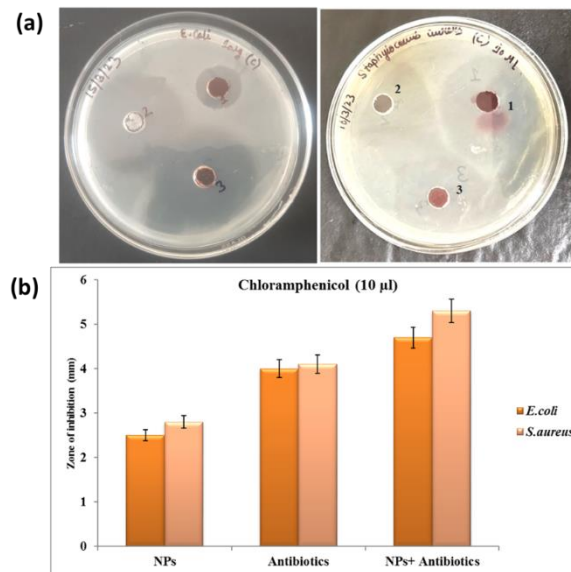


Figure 7. (a) Digital photographs of in vitro antibacterial activity of the chloramphenicol drug (10 μ L) loaded iron oxide nanoparticles against gram-negative (*E. coli*) and gram-positive (*S. aureus*) bacteria in Mueller-Hinton agar plates; (b) Zone of inhibition observed using the Chloramphenicol-coated Fe_2O_3 -NPs.

Thereafter, the conjugate contributes to cell annihilation primarily through two mechanisms: first, by inhibiting protein synthesis, and second, by damaging cell membranes. It thereby produces a highly efficient drug carrier [34]. All investigated species were found to exhibit a dose-dependent inhibitory effect of Fe_2O_3 -NPs. However, the assessment of increases in fold activity against *E. coli*, rather than *S. aureus*, showed that the maximal antibacterial activity of chloramphenicol increased with concentration from 10 to 30 μ L (see Figure 8).

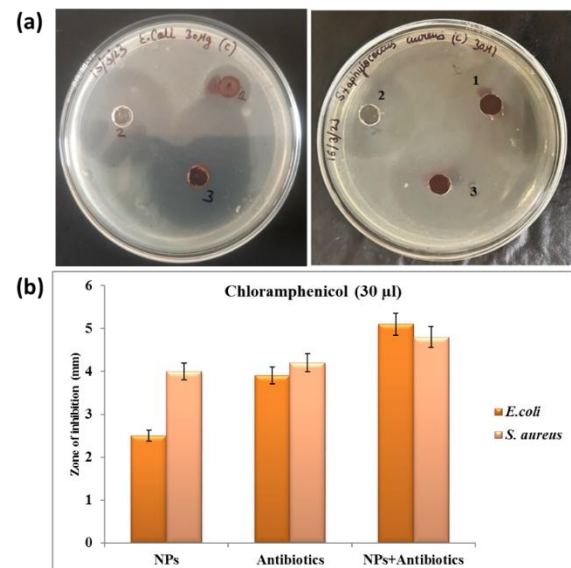


Figure 8. (a) Digital images of the antibacterial activity of the chloramphenicol medication (30 μ L) loaded iron oxide nanoparticles in Mueller-Hinton agar plates against gram-negative (*E. coli*) and gram-positive (*S. aureus*) bacteria; (b) Inhibition zone seen with chloramphenicol-coated Fe_2O_3 -NPs.

Similarly, Fe_2O_3 -NPs coated with the antibiotic streptomycin were also studied. Figures 9 and 10 show the antibacterial activity of Fe_2O_3 -NPs at different concentrations.

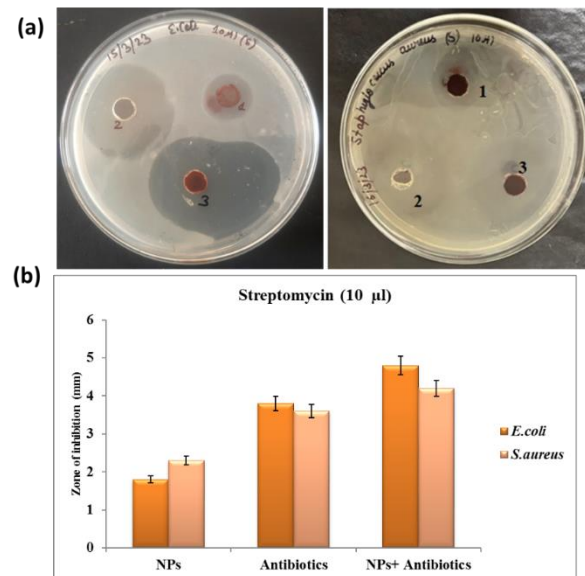


Figure 9. (a) Digital images showing the antibacterial activity of iron oxide nanoparticles loaded with the antibiotic streptomycin (10 µL) against *S. aureus* and *E. coli* bacteria on Mueller-Hinton agar plates; (b) Zone of inhibition shown with Fe₂O₃-NPs coated in streptomycin.

Streptomycin's most potent antibacterial action was also extremely significant against *S. aureus* and *E. coli*. *E. coli* showed the largest rise in fold area (0.96) for the drug streptomycin at 30 µL concentration, followed by *S. aureus*, which showed an increase in fold area (0.64) for the drug streptomycin, while a much smaller increase in fold area (0.26) was observed for *S. aureus* with chloramphenicol as a drug. Antibiotics chloramphenicol or streptomycin, without Fe₂O₃-NP encapsulation, were evaluated in vitro against *E. coli* and *S. aureus*, as shown in Figures 7-10.

The zone of inhibition for chloramphenicol coated with Fe₂O₃ nanoparticles was larger than that of the drug alone, as seen in Figures 7 and 8. Figures 9 and 10 show that similar results were obtained with streptomycin-coated Fe₂O₃ nanoparticles. As a result of the preceding research, it is clear that chloramphenicol- and streptomycin-coated iron oxide nanoparticles were particularly effective against both gram-positive and gram-negative bacteria, as indicated by a greater fold increase in the zone of inhibition diameter. Similar results have also been reported in the literature where iron oxide nanoparticles were synthesized by the coprecipitation method using various plant or fruit extracts as reducing agents [35–41].

The iron oxide nanoparticles, on the other hand, exhibited no negative or side effects on microbial activity. As a result, this property of Fe₂O₃-NPs as an effective drug carrier may be investigated further for drug delivery systems. Although the mechanism of contact between nanoparticles and the components of microorganisms' outer membranes is unknown, the particles' interactions with these components are likely to induce structural modifications or degradation. The mechanisms of the probable improvement in the antibacterial activity of iron oxide nanoparticle conjugates, in our opinion, remain an unanswered question that requires further investigation.

Based on the abovementioned discussion, it can be predicted that Fe₂O₃-NPs encapsulated with chloramphenicol and streptomycin antibiotic will become an efficient drug carrier against bacterial pathogens due to enhanced surface area, chemical stability, and adequate size of the produced NPs. However, extensive experimental trials on animals are needed before using Fe₂O₃-NPs as potential antimicrobial agents.

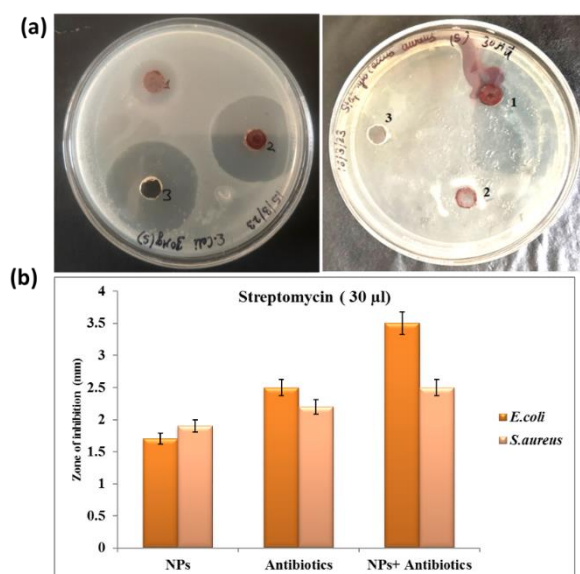


Figure 10. (a) Digital photographs of the antibacterial activity of iron oxide nanoparticles loaded with the antibiotic streptomycin (30 µL) against the microorganisms *S. aureus* and *E. coli* on Mueller-Hinton agar plates; (b) Streptomycin-coated Fe₂O₃-NPs are used to display the zone of inhibition.

4. Conclusions

In summary, nanoscale iron oxide particles were synthesized under atmospheric conditions using a simple, eco-friendly green synthesis method that employed ferric chloride hexahydrate as a precursor and various phytochemicals from sandalwood (*Santalum album*) extract as reducing and capping agents. Systematic analysis of iron oxide nanoparticles utilizing FESEM, EDX, XRD, FTIR, UV-Visible, and VSM validated their synthesis. Polyshaped iron oxide nanoparticles with a size of 42.9 ± 10 nm were synthesized. The magnetic properties of the manufactured Fe₂O₃-NPs were investigated at room temperature using a vibrating sample magnetometer, with a very low saturation magnetisation. The presence of detectable coercivity (H_c) and residual magnetism (M_r) in all samples demonstrates ferromagnetic ordering. The increased M_r and H_c of calcinated iron oxide samples as compared to nascent ones demonstrated that H_c and M_r are predominantly influenced by external characteristics such as crystallite size and particle formation, and so are tuned by calcination. As a result, the fluctuation in M_r and H_c demonstrates that magnetic characteristics vary with calcination temperature. In addition, drug nanofomulation was used to study in vitro antibacterial efficacy. To achieve this, streptomycin and chloramphenicol encapsulated Fe₂O₃-NPs were synthesized as nanoformulated antibiotics for in vitro antibacterial activity against gram-positive (*S. aureus*) and gram-negative (*E. coli*) bacteria on Mueller-Hinton agar plates. In comparison to streptomycin, the antibacterial activity of chloramphenicol was observed to be enhanced considerably in the presence of Fe₂O₃-NPs.

Author Contributions

Conceptualization, J.K.S. and M.K.B.; methodology, J.K.S., V.K., V.D.S., M.R., M.S., A.K., C.P., A.S., S.K., A.K.S., and M.K.B.; investigation, V.S., J.K.S., V.K., V.D.S., M.R., M.S., A.K., C.P., A.S., A.K.S., and M.K.B.; formal analysis, V.S., V.K., V.D.S., M.R., M.S., A.K., C.P., S.K., and A.K.S.; writing—original draft preparation, V.S.; writing—review and editing, M.K.B.; supervision, M.K.B. All authors have read and agreed to the published version of the manuscript.

Institutional Review Board Statement

Not applicable.

Informed Consent Statement

Not applicable.

Data Availability Statement

Data supporting the findings of this study are available upon reasonable request from the corresponding author.

Funding

This research received no external funding.

Acknowledgments

There is no acknowledgement.

Conflicts of Interest

The authors declare no conflict of interest.

References

1. Muzafar, W.; Kanwal, T.; Rehman, K.; Perveen, S.; Jabri, T.; Qamar, F.; Faizi, S.; Shah, M.R. Green Synthesis of Iron Oxide Nanoparticles Using Melia Azedarach Flowers Extract and Evaluation of Their Antimicrobial and Antioxidant Activities. *J. Mol. Struct.* **2022**, *1269*, 133824, <https://doi.org/10.1016/j.molstruc.2022.133824>.
2. Velsankar, K.; Parvathy, G.; Mohandoss, S.; Ravi, G.; Sudhahar, S. Echinochloa frumentacea grains extract mediated synthesis and characterization of iron oxide nanoparticles: A greener nano drug for potential biomedical applications. *J. Drug Deliv. Sci. Technol.* **2022**, *76*, 103799, <https://doi.org/10.1016/j.jddst.2022.103799>.
3. Areeshi, M.Y. Rice Straw Mediated Green Synthesis and Characterization of Iron Oxide Nanoparticles and Its Application to Improve Thermal Stability of Endoglucanase Enzyme. *Int. J. Food Microbiol.* **2022**, *374*, 109722, <https://doi.org/10.1016/j.ijfoodmicro.2022.109722>.
4. Lakshminarayanan, S.; Shereen, M.F.; Niraimathi, K.L.; Brindha, P.; Arumugam, A. One-Pot Green Synthesis of Iron Oxide Nanoparticles from Bauhinia Tomentosa: Characterization and Application towards Synthesis of 1, 3 Diolein. *Sci. Rep.* **2021**, *11*, 8643, <https://doi.org/10.1038/s41598-021-87960-y>.
5. Patiño-Ruiz, D.; Sánchez-Botero, L.; Tejada-Benitez, L.; Hinestroza, J.; Herrera, A. Green Synthesis of Iron Oxide Nanoparticles Using Cymbopogon Citratus Extract and Sodium Carbonate Salt: Nanotoxicological Considerations for Potential Environmental Applications. *Environ. Nanotechnol. Monit. Manag.* **2020**, *14*, 100377, <https://doi.org/10.1016/j.enmm.2020.100377>.
6. Bouafia, A.; Laouini, S.E. Green Synthesis of Iron Oxide Nanoparticles by Aqueous Leaves Extract of Mentha Pulegium L.: Effect of Ferric Chloride Concentration on the Type of Product. *Mater. Lett.* **2020**, *265*, 127364, <https://doi.org/10.1016/j.matlet.2020.127364>.
7. Pérez-Beltrán, C.H.; García-Guzmán, J.J.; Ferreira, B.; Estévez-Hernández, O.; López-Iglesias, D.; Cubillana-Aguilera, L.; Link, W.; Stănică, N.; Rosa da Costa, A.M.; Palacios-Santander, J.M. One-Minute and Green Synthesis of Magnetic Iron Oxide Nanoparticles Assisted by Design of Experiments and High Energy Ultrasound: Application to Biosensing and Immunoprecipitation. *Mater. Sci. Eng. C* **2021**, *123*, 112023, <https://doi.org/10.1016/j.msec.2021.112023>.
8. Karpagavinayagam, P.; Vedhi, C. Green Synthesis of Iron Oxide Nanoparticles Using Avicennia Marina Flower Extract. *Vacuum* **2019**, *160*, 286–292, <https://doi.org/10.1016/j.vacuum.2018.11.043>.

9. Selvaraj, R.; Pai, S.; Vinayagam, R.; Varadavenkatesan, T.; Kumar, P.S.; Duc, P.A.; Rangasamy, G. A Recent Update on Green Synthesized Iron and Iron Oxide Nanoparticles for Environmental Applications. *Chemosphere* **2022**, *308*, 136331, <https://doi.org/10.1016/j.chemosphere.2022.136331>.
10. Thomas Webster, T.J. Bactericidal Effect of Iron Oxide Nanoparticles on Staphylococcus Aureus. *Int. J. Nanomed.* **2010**, *2010*, 277-283, <https://doi.org/10.2147/IJN.S9220>.
11. Saqib, S.; Munis, M.F.H.; Zaman, W.; Ullah, F.; Shah, S.N.; Ayaz, A.; Farooq, M.; Bahadur, S. Synthesis, Characterization and Use of Iron Oxide Nano Particles for Antibacterial Activity. *Microsc. Res. Tech.* **2019**, *82*, 415–420, <https://doi.org/10.1002/jemt.23182>.
12. Li, D.; Shen, M.; Xia, J.; Shi, X. Recent Developments of Cancer Nanomedicines Based on Ultrasmall Iron Oxide Nanoparticles and Nanoclusters. *Nanomedicine* **2021**, *16*, 609–612, <https://doi.org/10.2217/nmm-2021-0033>.
13. Mathew, J.P.; Varghese, G.; Mathew, J. Effect of Post-Thermal Annealing on the Structural and Optical Properties of ZnO Thin Films Prepared from a Polymer Precursor. *Chin. Phys. B* **2012**, *21*, 078104, <https://doi.org/10.1088/1674-1056/21/7/078104>.
14. Dadfar, S.M.; Roemhild, K.; Drude, N.I.; von Stillfried, S.; Knüchel, R.; Kiessling, F.; Lammers, T. Iron Oxide Nanoparticles: Diagnostic, Therapeutic and Theranostic Applications. *Adv. Drug Deliv. Rev.* **2019**, *138*, 302–325, <https://doi.org/10.1016/j.addr.2019.01.005>.
15. Bender, P.; Fock, J.; Hansen, M.F.; Bogart, L.K.; Southern, P.; Ludwig, F.; Wiekhorst, F.; Szczerba, W.; Zeng, L.; Heinke, D. Influence of clustering on the magnetic properties and hyperthermia performance of iron oxide nanoparticles. *Nanotechnology* **2018**, *29*, 425705, <https://doi.org/10.1088/1361-6528/aad67d>.
16. Elsaidy, A.; Vallejo, J.P.; Salgueiriño, V.; Lugo, L. Tuning the Thermal Properties of Aqueous Nanofluids by Taking Advantage of Size-Customized Clusters of Iron Oxide Nanoparticles. *J. Mol. Liq.* **2021**, *344*, 117727, <https://doi.org/10.1016/j.molliq.2021.117727>.
17. Parveen, S.; Wani, A.H.; Shah, M.A.; Devi, H.S.; Bhat, M.Y.; Koka, J.A. Preparation, Characterization and Antifungal Activity of Iron Oxide Nanoparticles. *Microb. Pathog.* **2018**, *115*, 287–292, <https://doi.org/10.1016/j.micpath.2017.12.068>.
18. Nikam, A. V.; Prasad, B.L. V.; Kulkarni, A.A. Wet Chemical Synthesis of Metal Oxide Nanoparticles: A Review. *CrystEngComm* **2018**, *20*, 5091–5107, <https://doi.org/10.1039/C8CE00487K>.
19. Zhu, N.; Ji, H.; Yu, P.; Niu, J.; Farooq, M.; Akram, M.; Udego, I.; Li, H.; Niu, X. Surface Modification of Magnetic Iron Oxide Nanoparticles. *Nanomaterials* **2018**, *8*, 810, <https://doi.org/10.3390/nano8100810>.
20. Ashraf, I.; Singh, N.B.; Agarwal, A. Green Synthesis of Iron Oxide Nanoparticles Using Amla Seed for Methylene Blue Dye Removal from Water. *Mater. Today Proc.* **2023**, *72*, 311–316, <https://doi.org/10.1016/j.matpr.2022.07.404>.
21. Parmanik, A.; Bose, A.; Ghosh, B.; Paul, M.; Ito, A.; Biswas, S.; Arakha, M. Development of Triphala Churna Extract Mediated Iron Oxide Nanoparticles as Novel Treatment Strategy for Triple Negative Breast Cancer. *J. Drug Deliv. Sci. Technol.* **2022**, *76*, 103735, <https://doi.org/10.1016/j.jddst.2022.103735>.
22. Singh, M.; Manikandan, S.; Yadav, M.; Kumar, S.; Sehrawat, N.; Meashi, V.; Diksha, D.; Sharma, P.; Sharma, A.K. Bio-Functionalized Gold Nanoparticles: A Potent Probe for Profound Antibacterial Efficiency through Drug Delivery System. *Asian J. Biol. Life Sci.* **2020**, *9*, 139–144, <https://doi.org/10.5530/ajbls.2020.9.21>.
23. Zachariah, M.R.; Aquino, M.I.; Shull, R.D.; Steel, E.B. Formation of Superparamagnetic Nanocomposites from Vapor Phase Condensation in a Flame. *Nanostructured Mater.* **1995**, *5*, 383–392, [https://doi.org/10.1016/0965-9773\(95\)00260-L](https://doi.org/10.1016/0965-9773(95)00260-L).
24. Cui, H.; Liu, Y.; Ren, W. Structure Switch between α -Fe₂O₃, γ -Fe₂O₃ and Fe₃O₄ during the Large Scale and Low Temperature Sol–Gel Synthesis of Nearly Monodispersed Iron Oxide Nanoparticles. *Adv. Powder Technol.* **2013**, *24*, 93–97, <https://doi.org/10.1016/j.apt.2012.03.001>.
25. Kumar, A.; Gangawane, K.M. Effect of Precipitating Agents on the Magnetic and Structural Properties of the Synthesized Ferrimagnetic Nanoparticles by Co-Precipitation Method. *Powder Technol.* **2022**, *401*, 117298, <https://doi.org/10.1016/j.powtec.2022.117298>.
26. Shabani, N.; Javadi, A.; Jafarizadeh-Malmiri, H.; Mirzaie, H.; Sadeghi, J. Potential Application of Iron Oxide Nanoparticles Synthesized by Co-Precipitation Technology as a Coagulant for Water Treatment in Settling Tanks. *Mining, Metall. Explor.* **2021**, *38*, 269–276, <https://doi.org/10.1007/s42461-020-00338-y>.
27. Sundaram, N.M.; Murugesan, S. Preparation and Characterization of an Iron Oxide-Hydroxyapatite Nanocomposite for Potential Bone Cancer Therapy. *Int. J. Nanomed.* **2015**, *10*, 99-106, <https://doi.org/10.2147/IJN.S79985>.

28. Alias, S.S.; Ismail, A.B.; Mohamad, A.A. Effect of PH on ZnO Nanoparticle Properties Synthesized by Sol–Gel Centrifugation. *J. Alloys Compd.* **2010**, *499*, 231–237, <https://doi.org/10.1016/j.jallcom.2010.03.174>.
29. Mazrouaa, A.M.; Mohamed, M.G.; Fekry, M. Physical and Magnetic Properties of Iron Oxide Nanoparticles with a Different Molar Ratio of Ferrous and Ferric. *Egypt. J. Pet.* **2019**, *28*, 165–171, <https://doi.org/10.1016/j.ejpe.2019.02.002>.
30. Slimani, S.; Meneghini, C.; Abdolrahimi, M.; Talone, A.; Murillo, J.P.M.; Barucca, G.; Yaacoub, N.; Imperatori, P.; Illés, E.; Smari, M. Spinel iron oxide by the co-precipitation method: Effect of the reaction atmosphere. *Appl. Sci.* **2021**, *11*, 5433, <https://doi.org/10.3390/app11125433>.
31. Pankove, J.I.; Kiewit, D.A. Optical Processes in Semiconductors. *J. Electrochem. Soc.* **1972**, *119*, 156C, <https://doi.org/10.1149/1.2404256>.
32. Harris, T.V.; Szilagyi, R.K. Iron–Sulfur Bond Covalency from Electronic Structure Calculations for Classical Iron–Sulfur Clusters. *J. Comput. Chem.* **2014**, *35*, 540–552, <https://doi.org/10.1002/jcc.23518>.
33. Xiao, L.; Liu, F.; Kumar, P.S.; Wei, Y.; Liu, J.; Han, D.; Shan, S.; Wang, X.; Dang, R.; Yu, J. Rapid Removal of Chloramphenicol via the Synergy of Geobacter and Metal Oxide Nanoparticles. *Chemosphere* **2022**, *286*, 131943, <https://doi.org/10.1016/j.chemosphere.2021.131943>.
34. Bloemen, M.; Denis, C.; Peeters, M.; De Meester, L.; Gils, A.; Geukens, N.; Verbiest, T. Antibody-Modified Iron Oxide Nanoparticles for Efficient Magnetic Isolation and Flow Cytometric Determination of *L. Pneumophila*. *Microchim. Acta* **2015**, *182*, 1439–1446, <https://doi.org/10.1007/s00604-015-1466-z>.
35. Rufus, A.; N., S.; Philip, D. Synthesis of Biogenic Hematite (α -Fe₂O₃) Nanoparticles for Antibacterial and Nanofluid Applications. *RSC Adv.* **2016**, *6*, 94206–94217, <https://doi.org/10.1039/C6RA20240C>.
36. Pallela, P.N.V.K.; Ummey, S.; Ruddaraju, L.K.; Gadi, S.; Cherukuri, C.S.; Barla, S.; Pammi, S.V.N. Antibacterial Efficacy of Green Synthesized α -Fe₂O₃ Nanoparticles Using *Sida Cordifolia* Plant Extract. *Heliyon* **2019**, *5*, e02765, <https://doi.org/10.1016/j.heliyon.2019.e02765>.
37. Patra, J.K.; Ali, M.S.; Oh, I.-G.; Baek, K.-H. Proteasome Inhibitory, Antioxidant, and Synergistic Antibacterial and Anticandidal Activity of Green Biosynthesized Magnetic Fe₃O₄ Nanoparticles Using the Aqueous Extract of Corn (*Zea Mays* L.) Ear Leaves. *Artif. Cells Nanomed. Biotechnol.* **2017**, *45*, 349–356, <https://doi.org/10.3109/21691401.2016.1153484>.
38. Vasantharaj, S.; Sathiyavimal, S.; Senthilkumar, P.; LewisOscar, F.; Pugazhendhi, A. Biosynthesis of Iron Oxide Nanoparticles Using Leaf Extract of *Ruellia Tuberosa*: Antimicrobial Properties and Their Applications in Photocatalytic Degradation. *J. Photochem. Photobiol. B Biol.* **2019**, *192*, 74–82, <https://doi.org/10.1016/j.jphotobiol.2018.12.025>.
39. Mousavi, S.M.; Hashemi, S.A.; Zarei, M.; Bahrani, S.; Savardashtaki, A.; Esmaeili, H.; Lai, C.W.; Mazraedoost, S.; Abassi, M.; Ramavandi, B. Data on Cytotoxic and Antibacterial Activity of Synthesized Fe₃O₄ Nanoparticles Using *Malva Sylvestris*. *Data Br.* **2020**, *28*, 104929, <https://doi.org/10.1016/j.dib.2019.104929>.
40. Bashir, M.; Ali, S.; Farrukh, M.A. Green Synthesis of Fe₂O₃ Nanoparticles from Orange Peel Extract and a Study of Its Antibacterial Activity. *J. Korean Phys. Soc.* **2020**, *76*, 848–854, <https://doi.org/10.3938/jkps.76.848>.
41. Ahmadi, S.; Fazilati, M.; Nazem, H.; Mousavi, S.M. Green Synthesis of Magnetic Nanoparticles Using *Satureja Hortensis* Essential Oil toward Superior Antibacterial/Fungal and Anticancer Performance. *Biomed Res. Int.* **2021**, *2021*, 1–14, <https://doi.org/10.1155/2021/8822645>.

Publisher’s Note & Disclaimer

The statements, opinions, and data presented in this publication are solely those of the individual author(s) and contributor(s) and do not necessarily reflect the views of the publisher and/or the editor(s). The publisher and/or the editor(s) disclaim any responsibility for the accuracy, completeness, or reliability of the content. Neither the publisher nor the editor(s) assume any legal liability for any errors, omissions, or consequences arising from the use of the information presented in this publication. Furthermore, the publisher and/or the editor(s) disclaim any liability for any injury, damage, or loss to persons or property that may result from the use of any ideas, methods, instructions, or products mentioned in the content. Readers are encouraged to independently verify any information before relying on it, and the publisher assumes no responsibility for any consequences arising from the use of materials contained in this publication.